JOURNAL OF MATERIALS SCIENCE **40** (2005) 387–398

Structural, electrical and magnetic properties of copper-cadmium ferrites prepared from metal oxalates

M. A. GABAL*
Chemistry Department, Faculty of Science, Benha University, Benha, Egypt
E-mail: mgabalabdo@yahoo.com

M. A. AHMED
Physics Department, Faculty of Science, Cairo University, Giza, Egypt

Seven samples of the system $Cu_{1-x}Cd_xFe_2O_4$ were prepared by thermal decomposition of mixed metal oxalates with $x = 0.0, 0.1, 0.3, 0.5, 0.7, 0.9$ and 1.0. The formation of the ferrispinel was studied by XRD, FT-IR, Mössbauer spectroscopy, electrical conductivity and magnetic susceptibility measurements. XRD showed single cubic spinel phase for all the samples except for $CuFe_2O_4$ sample which shows a tetragonal structure. An increase in the lattice parameter of the ferrispinel was observed with increasing the cadmium content. The temperature variation of ac conductivity showed four definite regions with three transitions which attribute to the change in the conduction mechanism with increasing temperature. Magnetic properties of the sample with $x \leq 0.5$ showed a decrease in the effective magnetic moment with the increase in the cadmium content which means that the ferromagnetics are widely separated and enclosed by non-magnetic cadmium ions. A well defined hyperfine Zeeman spectrum is observed for samples with $x \geq 0.3$ at room temperature and resolved into two sextets corresponding to the octahedral and tetrahedral sites. The propable ionic configuration of the system proposed is $(Cd_xCu_yFe_{1-x-y})[Cu_{1-x-y}Fe_{1+x+y}]O_4$.

1. Introduction

Among the magnetic materials, the so called soft ferrites not only represent an active field of research and development, but also an important commercial activity. Indeed, owing to their high electrical resistivity (over on million times that of equivalent magnetic alloys) that implies low losses due to parasitic currents, and to their susceptibility, they are preferred in applications ranging from transformers to magnetic heads. In addition, their high permeability in the r.f. frequency region, make polycrystalline ferrites suitable for an increasing number of electron devices [1].

Amongst ferrites, copper ferrite is unique in the context of establishing mutual relationships between the magnetic and structural properties. This ferrite exist in two crystallographic forms, the tetragonal distorted with axial ratio $c/a > 1$ below 1170°C and cubic above this temperature [2].

Diamagnetic substitution in simple and mixed ferrites has received a lot of attention over the past years [3–7]. The preference of nonmagnetic ions in spinel was found to alter their magnetic and electrical properties, and studies have revealed useful information on the nature of the exchange interaction, direction of magnetization, cation distribution, spin canting etc. Such isomorphous substitution in iron oxides are particularly apparent in their Mössbauer spectra, since these will drastically reduce magnetic interactions, resulting in lower magnetic ordering temperature and decreases magnetic field supertransfer [8].

The composition dependence of some physical parameters such as the density, lattice parameters, porosity, percentage shrinkage, electrical resistivity and thermo electric power of $Cu_{1-x}Cd_xFe_2O_4$ ferrospinel (with $0 \leq x \leq 1$) were studied by Mazen *et al.* [3]. ac electrical parameters such as the dielectric constant (ε_r) and the loss tangent ($\tan\delta$) for slow-cooled and air quenched samples of $Cu_{1-x}Cd_xFe_2O_4$ system (where x varies from 0 to 1) at 400, 600 and 800°C have been studied as a function of frequency [4]. The cation distribution in $Cu_{1-x}Cd_xFe_2O_4$ ($0.2 \leq x \leq 1.0$) ferrite system, estimated using X-ray diffraction technique supports the cation distribution predicted by the magnetization method [5].

The standard ceramic technique is known to be the most famous one for the preparation of copper-cadmium ferrite [3–7], however, there is no currently

*Author to whom all correspondence should be addressed.

any work in the literature on the preparation of this mixed ferrite from oxalate precursors.

In the present investigation we have prepared the compounds of the system $Cu_{1-x}Cd_xFe_2O_4$ ($0 \leq x \leq 1$) through the thermal decomposition of mixed metal oxalates. We attempt to determine the effect of copper ferrite spinel formation and the role of cadmium content on structural, electrical, and magnetic properties of these ferrospinels.

2. Experimental details

2.1. Synthesis of precursors

Individual metal oxalates; CuC_2O_4, $CdC_2O_4 \cdot 3H_2O$ and $FeC_2O_4 \cdot 2H_2O$ were prepared by coprecipitation with high purity oxalic acid from aqueous solution of the AnalaR salt sulphates. The obtained precipitates were filtered, washed by distilled water until sulphate-ions free and dried in air.

The solid state oxalates mixtures were prepared using the impregnation technique [9]. Stoichiometric ratios of the individual oxalates were thoroughly mixed in a porcelain morter. During vigorous stirring, drops of bi-distilled water were added to assure complete homogeneity. The wetted oxalates mixture were then dried in an electrical oven.

2.2. Synthesis of copper cadmium ferrites

For the synthesis of $Cu_{1-x}Cd_xFe_2O_4$ ferrites ($0 \leq x \leq 1$), as evident from DTA-TG experiment, the above oxalates mixtures were decomposed and calcined in a muffle furnace at 1000°C for 4 h using platinum crucible under static air atmosphere. The samples were then air-quenched to room temperature and stored in a desiccator.

2.3. Techniques

DTA-TG behavior of mixed oxalates was investigated using a Shimadzu DT-60 thermal analyzer (Japan). The temperature was raised up to 1000°C under 1 atm pressure in air flow (30 ml min^{-1}) at heating rate of 5°C min^{-1}. α-Al_2O_3 powder (Shimadzu) was used as the reference material for DTA measurements and the sample weight in the PT-cell was about 10 mg.

X-ray powder diffraction measurements were obtained using a Philips PW 1370 diffractometer at ambient temperature using monochromated Cu $K_{\alpha 1}$ radiation ($\lambda = 1.5406$ Å).

Fourier transform-infrared spectra were recorded at room temperature in the frequency range 1000–200 cm^{-1} employing KBr disc technique using a Jasco FT-IR 310 spectrophotometer (Japan).

Mössbauer spectra of the ferrite samples were measured with a time mode spectrometer, calibrated with a high purity natural iron foil of 10 mg cm^{2-} thickness, using a constant acceleration deriver and personal computer analyzer (PCAII-card) coupled to a 1024 multichannel analyzer. A 50 mCi^{57} Co in Rh matrix was used as the radioactive source. Experimental data were analyzed using the least square fitting "Mos-90" computer program [10].

For electrical properties measurements, the ferrite samples in a powdered form were compressed to pellets of 1 cm diameter and about 1 mm thickness. The pressure used was 2 tons cm^{-2}. After calcining the pellets at 900°C for 2 h, the two surfaces of each one were polished and coated with silver paint (BDH) and tested for Ohmic contact. The real part of the dielectric constant (ε') and ac conductivity were measured, by a Hioki LCR bridge model 3531 (Japan) using the two probe method [11], at different frequencies (10–5000 kHz) as a function of temperature. The temperature of the sample was measured using a thermocouple type K which is connected to a digital thermometer.

The magnetic susceptibility of the investigated samples at different temperatures as a function of different magnetic field intensities was measured using Faraday's method in which the sample was inserted at the point of maximum force.

3. Results and discussion

3.1. Thermal decomposition course of mixed metal oxalates

The thermal decomposition studies of the oxalates mixtures shows that all the mixtures dehydrate and decompose in the temperature range from 60 to 370°C. A typical DTA-TG thermogram for the thermal decomposition of CuC_2O_4-$CdC_2O_4 \cdot 3H_2O$-$FeC_2O_4 \cdot 2H_2O$ (0.5:0.5:2 mole ratios) in air is shown in Fig. 1. It can be observed that the mixture loses its weight in three well-defined steps giving at complete decomposition a total weight loss of 53% which corresponds to the formation of corresponding copper cadmium ferrite; $Cu_{0.5}Cd_{0.5}Fe_2O_4$ (calculated weight loss = 53.3%). The first step starts at 60°C and characterized by a sharp endothermic DTA peak at 105°C. The weight loss that accompanied this step amounts to 4.7% and attributed to the dehydration of $CdC_2O_4 \cdot 3H_2O$. The mixture is thermally stable up to 157°C after which the main decomposition step occurs. This step exhibits a weight loss of 36% at 250°C which closely corresponds to the complete decomposition of $FeC_2O_4 \cdot 2H_2O$ with the formation of Fe_2O_3 (theoretical weight loss = 35.5%). This step showed no separate anhydrous oxalate plateau. The sharp endothermic DTA peak at 214°C was swamped by the large exothermic decomposition peak occurred at 230°C. The third step follows immediately after the completion of the second step and accounts for the exothermic decomposition (exothermic DTA maximized at 328°C) of CuC_2O_4 and CdC_2O_4 with the formation of CuO and CdO, respectively. This step is associated with 12.3% weight loss at 364°C which agrees with the calculated weight loss of 12.8%. No further weight loss was observed even by rising the temperature up to 1000°C.

The decomposition behavior of each metal oxalate in this decomposition course resemble that for its individual metal oxalate [12, 13]. This suggests the absence of any solid solution formed between the respective metal oxalates since each one behaves as it is present alone in the mixture.

3.2. Characterization of $Cu_{1-x}Cd_xFe_2O_4$

3.2.1. X-ray diffraction studies

The X-ray diffraction at all the composition of samples under investigation indicates the formation of a single

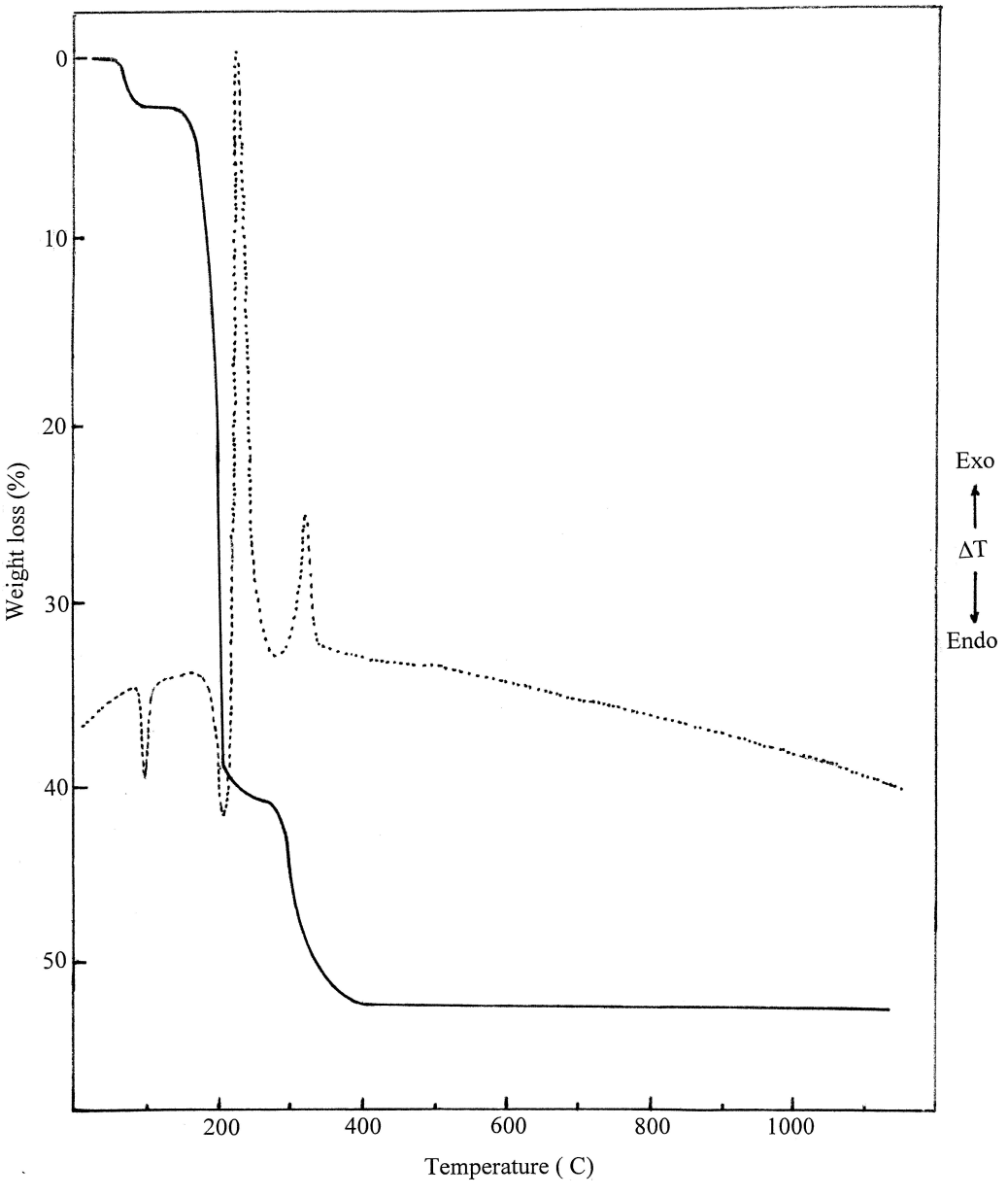

Figure 1 DTA-TG curves of $CuC_2O_4{\cdot}2H_2O$-$CdC_2O_4{\cdot}3H_2O$-$FeC_2O_4{\cdot}2H_2O$ (0.5:0.5:2 mole ratios) mixture in air at a specified heating rate of 5°C min^{-1}.

spinel phase that has cubic structure with no additional lines corresponding to any other phases. Exception is for the sample with $x = 0$ i.e., $CuFe_2O_4$ sample which shows a tetragonal crystal structure. This result agrees well with that obtained by Kulkarni and Vainganker [4]. The tetragonal distortion is due to Jahn-Teller effect of Cu^{2+} ions located in the octahedral sites of spinel with a large concentration [8].

Fig. 2 shows the X-ray powder diffraction of the investigated samples. The experimentally observed d-spacing values and relative intensities are in well agreement with those reported in the ASTM powder diffraction files [14]. The lattice parameters are obtained by fitting at least seven diffraction peaks using standard least square methods and tabulated in Table I. Using lattice parameter values, the X-ray density (D_x) of all the investigated samples were calculated and reported in Table I. The lattice parameter constant values are in the expected range with the lattice constant of $CuFe_2O_4$ [8] and $CdFe_2O_4$ [7] at either end. The variation of lattice parameter (a) as a function of cadmium substitution (x) is represented in Fig. 3a. It is obvious that the lattice parameter increases linearly according to Vegard's law [15] with the increase of cadmium content. This could be attributed, as expected, to the large ionic radius of Cd^{2+} (0.78 Å) which when substituted in the lattice resides on the tetrahedral site and replaces the smaller Cu^{2+} (0.57 Å) or Fe^{3+} (0.49 Å) ions from the tetrahedral to the octahedral site [5]. According to Cervinka

TABLE I Characterization data of $Cu_{1-x}Cd_xFe_2O_4$ system

Cd content (x)	Lattice parameter (Å)	D_x (gm cm^{-3})	ν_1 (cm^{-1})	ν_2 (cm^{-1})
0.0	$a = 8.278$ $c = 8.686$	5.077	586	385
0.1	8.345	5.580	577	380
0.3	8.434	5.621	571	378
0.5	8.473	5.758	563	378
0.7	8.528	5.856	561	377
0.9	8.580	5.959	548	376
1.0	8.614	5.986	541	376

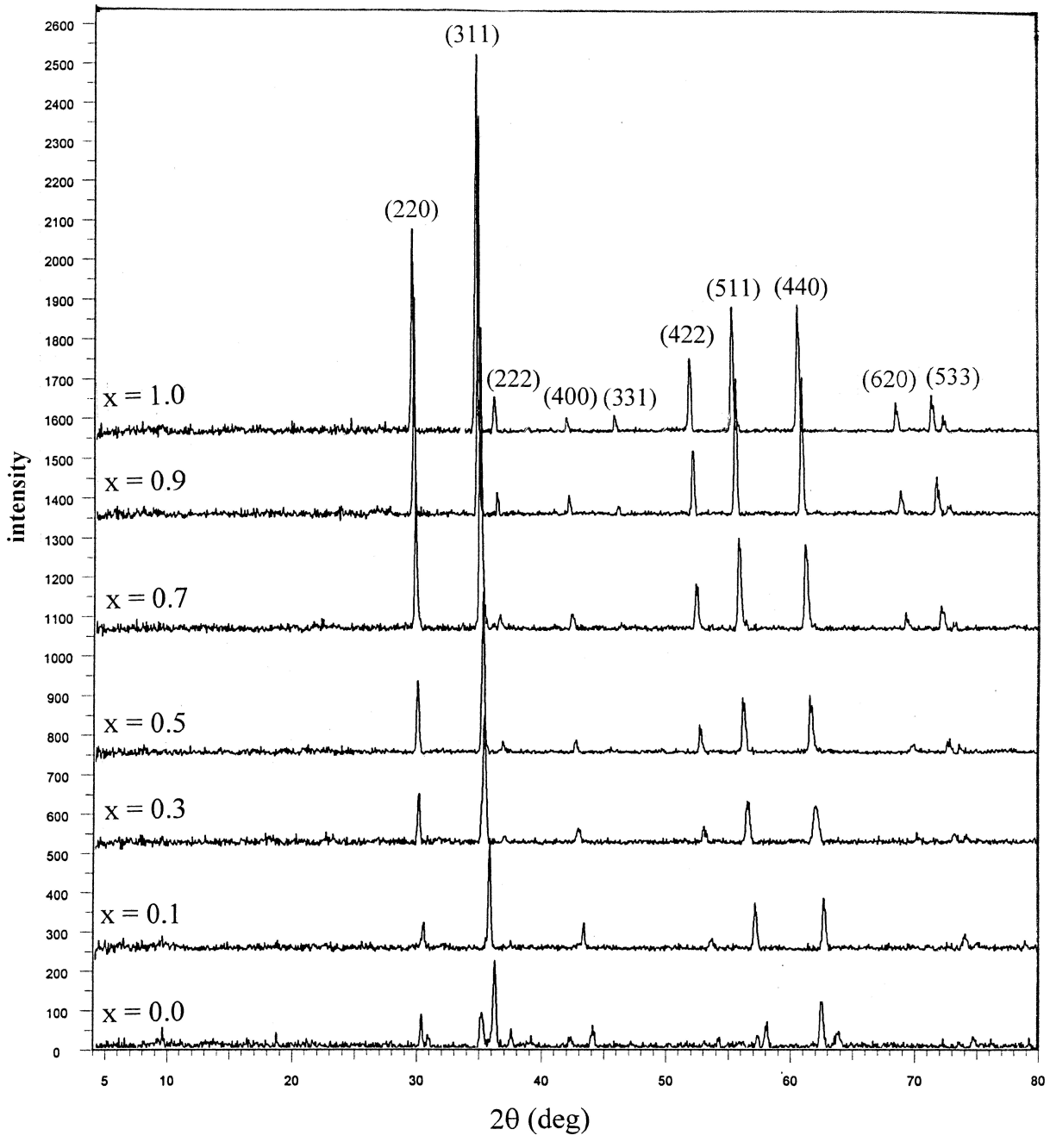

Figure 2 Characteristic parts of XRD patterns of $Cu_{1-x}Cd_xFe_2O_4$ system.

et al. [16] the intensities of (220) and (422) planes are mostly sensitive to cations on tetrahedral site while that of (400) plane depend on cations on the octahedral site. The ratios I_{222}/I_{400} and I_{422}/I_{400} as a function of cadmium content are represented in Fig. 3b. The increasing trend of this graph with x supports the occupancy of Cd^{2+} ions on the tetrahedral site.

The X-ray density (D_x) values reported in Table I was found to increase with increasing x. This was expected since the larger cadmium atom is heavier than the smaller copper atom, and this increase in weight and decrease in size causes an increase in X-ray density with the substitution of cadmium.

3.2.2. FT-IR spectral studies

FT-IR spectra of $Cu_{1-x}Cd_xFe_2O_4$ samples show two strong bands ν_1 and ν_2 near about 600 and 400 cm^{-1}, respectively. The band positions are listed in Table I. Waldron [17] attributed the band ν_1 at around 600 cm^V to the intrinsic vibration of tetrahedral metal-oxygen complexes and the band ν_2 at around 400 cm^{-1} to the intrinsic vibration of octahedral complexes. The absence of the low frequency bands in our compounds suggests that the lattice vibrations responsible for these bands are very weak.

The band appearing at 586 cm^{-1} for $CuFe_2O_4$ shows an obvious red shift on addition of cadmium in the system and changes to $CdFe_2O_4$. Variation of ν_1 and ν_2 bands with the cadmium concentration (x) is shown in Fig. 3c and d, respectively. From the figure it is clear that, ν_1 increases with increasing x while, ν_2 slightly changes.

3.2.3. ^{57}Fe Mössbauer spectroscopy

The room temperature Mössbauer spectra of $CuFe_2O_4$, $CdFe_2O_4$ and their mixed ferrites are shown in Fig. 4. The spectral parameters such as isomer shift (δ),

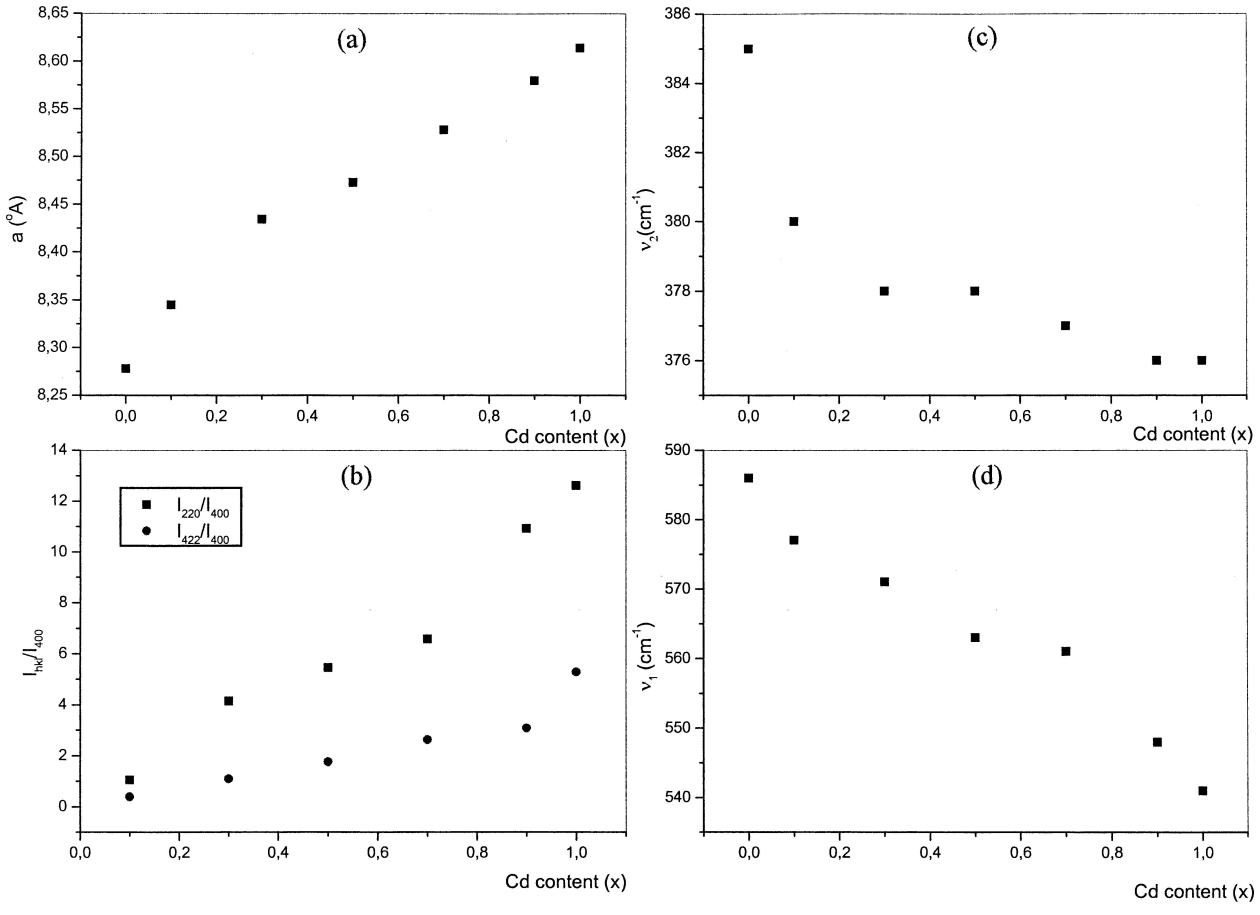

Figure 3 (a) Variation of lattice parameter (a) as a function of Cd content, (b) The ratio of observed intensities of X-ray line I_{220}/I_{222} and I_{422}/I_{222} as a function of Cd content, (c) Variation of ν_1 FT-IR band with composition, and (d) Variation of ν_2 FT-IR band with composition.

quadrupole splitting (ΔE_Q) and hyperfine fields (H_n) at tetrahedral and octahedral sites are computed and summarized in Table II. the black dots represent experimental points and the continuous lines through the data points are results of the least square fit to the data.

For the stoichiometric compound $CuFe_2O_4$, the Mössbauer spectrum consists of two clearly splitted Zeeman sextets due to Fe^{3+} at tetrahedral and octahedral sites. The samples with composition $x = 0.1$ and 0.3 exhibit more broadened Zeeman patterns. Such broadening is expected since the presence of nonmagnetic Cd^{2+} ions in the neighborhood of iron nuclei will vary the hyperfine interactions and influence the Mössbauer patterns.

A relaxed spectrum was obtained for sample with $x = 0.5$. The dominant spin lattice relaxation in the spectrum may be attributed to the presence of the tetrahedral quadrupole interaction due to replacement of Fe^{3+} ions by Cd^{2+} ions in the tetrahedral site. The spectrum was fitted with one sextet due to Fe^{3+} ions at one of the two crystallographic distinct sites and was attributed to the octahedral site on the basis of the isomer shift and the hyperfine field values.

The samples with cadmium concentration higher than 0.5 are paramagnetic at room temperature as can be seen from Fig. 4. This is due to the predominance of the paramagnetic phase in these samples. In a deeper explanation for this behavior, a ferromagnetic region exist instead of ferrimagnetic one, which are separated magnetically from the matrix by diamagnetic Cd^{2+} ions. The line width of the paramagnetic doublet was found to decrease with increasing Cd-content (Table II).

TABLE II Mössbauer parameters of $Cu_{1-x}Cd_xFe_2O_4$ system

Cd content (x)	Site	Area (%)	Isomer shift (δ) ($\pm$0.02 mm s^{-1})	Quadrupole splitting (ΔE_Q) ($\pm$0.02 mm s^{-1})	Line width (Γ mm s^{-1})	Hyperfine field (H) ($\pm$2kOe)
0.0	A	80	0.43	0.02	0.47	479
	B	20	0.52	0.08	0.63	507
0.1	A	70	0.40	0.04	0.57	468
	B	30	0.50	0.06	0.83	474
0.3	A	50	0.43	0.06	0.94	392
	B	50	0.46	0.08	1.67	442
0.5	B	–	0.45	0.05	3.60	304
0.7	–	–	0.43	0.82	0.51	–
0.9	–	–	0.43	0.81	0.37	–
1.0	–	–	0.44	0.79	0.36	–

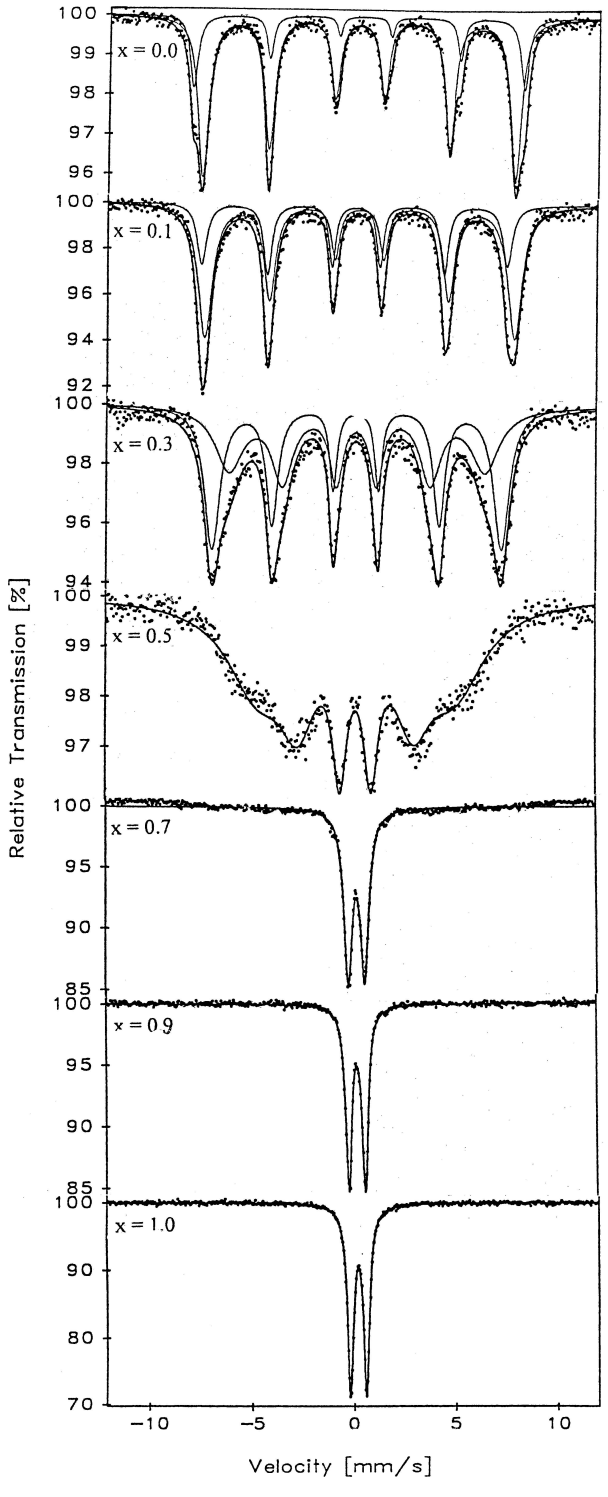

Figure 4 The Mössbauer spectra at room temperature of $Cu_{1-x}Cd_xFe_2O_4$ system.

The fraction of iron at the two distinct crystallographic sites can be determined from the Mössbauer spectrum by knowing the area under the resonance lines due to these ions. From the literature it is well known that, copper ions preferentially gets distributed among tetrahedral and octahedral sites. Kolekar *et al.* [18] reported that copper ferrite is 81% inverse spinel. Narayanasamy *et al.* [19] suggest a cation distribution of $(Cu_{0.22}Fe_{0.78})[Cu_{0.78}Fe_{1.22}]O_4$ for copper ferrite. In consistent with these results, the areas under the two Zeeman subspectra of copper ferrite in the present work (Table II) gave a cation distribution as: $(Cu_{0.20}Fe_{0.80})[Cu_{0.80}Fe_{1.20}]O_4$.

The cation distribution estimated using the Mössbauer subspectra areas for samples with $x = 0.1$ and 0.3 are: $(Cd_{0.1}Cu_{0.20}Fe_{0.70})[Cu_{0.70}Fe_{1.30}]O_4$ and $(Cd_{0.30}Cu_{0.20}Fe_{0.50})[Cu_{0.50}Fe_{1.50}]O_4$, respectively which suggests that Cd^{2+} ions have a special preference for the tetrahedral coordination as previously suggested using X-ray diffraction.

From the above results, the cation distribution formula that can be used to describe the system can be written as: $(Cd_xCu_yFe_{1-x-y})[Cu_{1-x-y}Fe_{1+x+y}]O_4$ where x denotes the amount of substituted cadmium, y is the normalcy of copper ions and the inversion parameter $(\delta) = 1 - x - y$. The deduced values for the cation distribution of the system are given in Table III.

From Table II it is clear that, there is no significant change of isomer shift values with cadmium content in the spinel system with $x \leq 0.5$. This means that the s electron charge distribution of Fe^{3+} ions is negligibly influenced by cadmium substitution. Also, it is clearly observed that the values of quadrupole splitting are negligibly small. This could be explained due to the overall cubic symmetry of the spinel ferrite and randomness of chemical disorder, there will be equal probability for small quadrupole splitting of opposite signs. Hence, the centers of the Zeeman lines will not change, and consequently there will be no net observed quadrupole splitting. The hyperfine field at either sites was found to decrease as the cadmium content increases. This demonstrates a reduction in ferrimagnetic behavior with increasing x.

Depending on the cation distribution estimated using the Mössbauer technique, the values of oxygen positional parameter (u) and the degree of inversion (γ) were calculated and summarized in Table III. For a given spinel compound, the anion sublattice expands or contracts on varying oxygen parameter until the tetrahedral and the octahedral site volumes match the radii of the constituent cations. From Table III, it can be noticed that, the oxygen parameter increases with increasing x and is found to be close to the reported values for the end members ($u = 0.381$ and 0.391 for $CuFe_2O_4$ and $CdFe_2O_4$, respectively) [5]. The inversion parameter (γ), defined as the total fraction of divalent ions lodged in the octahedral site, was found to decrease and going towards complete inversion at $x = 0.9$.

Using the experimental values of the lattice and oxygen parameters and the following Equations 1–5 given below [20], the interionic distances and the radii of the tetrahedral and octahedral bonds (r_A and r_B) are calculated and listed in Table III.

$$d_{AX} = \sqrt{3}\left(u - \frac{1}{u}\right)a \quad \text{(tet. Bond)} \tag{1}$$

$$d_{BX} = \left(3u^2 - \frac{11u}{4} + \frac{43}{6u}\right)^{1/2} a \quad \text{(oct. bond)} \tag{2}$$

$$d_{xX} = \sqrt{2}\left(2u - \frac{1}{2}\right)a \quad \text{(tet. Edge)} \tag{3}$$

$$d_{XX} = \sqrt{2}(1 - 2u)a \quad \text{(shared oct. edge)} \tag{4}$$

TABLE III Cation distribution, oxygen parameter, inversion parameter and cation-anion distance of $Cu_{1-x}Cd_xFe_2O_4$ system

Cation distribution	u	γ	r_A (Å)	r_B (Å)	Tet. bond (Å)	Oct. bond (Å)	Tet. edge (Å)	Oct. edge (Å)	
								Shared	Unshared
$(Cu_{0.2}Fe_{0.8})[Cu_{0.8}Fe_{1.2}]O_4$	0.381	0.8	0.506	1.358	1.865	2.006	3.046	2.767	2.908
$(Cd_{0.1}Cu_{0.2}Fe_{0.7})[Cu_{0.7}Fe_{1.3}]O_4$	0.382	0.7	0.535	1.350	1.908	2.029	3.116	2.785	2.953
$(Cd_{0.3}Cu_{0.2}Fe_{0.5})[Cu_{0.5}Fe_{1.5}]O_4$	0.385	0.5	0.593	1.333	1.972	2.030	3.220	2.743	2.987
$(Cd_{0.5}Cu_{0.2}Fe_{0.3})[Cu_{0.3}Fe_{1.7}]O_4$	0.388	0.3	0.651	1.316	2.025	2.159	3.307	2.684	3.003
$(Cd_{0.7}Cu_{0.2}Fe_{0.1})[Cu_{0.1}Fe_{1.9}]O_4$	0.391	0.1	0.709	1.299	2.083	2.004	3.401	2.629	3.028
$(Cd_{0.9}Cu_{0.1})[Fe_2]O_4$	0.393	0.0	0.759	1.290	2.125	2.002	3.470	2.597	3.049
$(Cd)[Fe_2]O_4$	0.394	0.0	0.780	1.290	2.149	2.003	3.509	2.583	3.063

$$d_{XX} = \left(4u^2 - 3u + \frac{11}{16}\right)^{1/2} a \quad \text{(unshared oct. edge)} \tag{5}$$

The radius of tetrahedral and octahedral sites were calculated for the different spinels and given in Table III. From the results it is clear that, the radius of the tetrahedral site becomes larger on addition of cadmium ions and that of the octahedral site slightly changed. This was ascribed to the preference of the cadmium ions with larger ionic radius for the tetrahedral coordination. This may also be the reason for explaining the variance of ν_1 and ν_2 band position with varying the cadmium content (Fig. 3c and d).

3.2.4. Electrical properties studies

Fig. 5 shows a typical curve correlating the ac conductivity and reciprocal of absolute temperature for the ferrite samples with different cadmium content at different applied frequency. From the figure it is clear that four regions intersecting at three transition temperatures are obtained, one of them is distinguished as the Curie point (T_C). The first and the last regions are nearly the same, clarifying the metallic behavior of the investigated samples in the low and very high temperature regions. The thermal energy in the first region is not enough to liberate charge carriers and consequently the conductivity is hardly changed with temperature. In the last region the large thermal energy causes a large lattice vibration and the scattering of the charge carriers due to their collision with the vibrating lattice was expected to damp the mobility up to the extent at which it becomes constant and giving rise to a constant conductivity. In the intermediate part, two straight lines were obtained at all the applied frequencies. The first one at the low temperature region represents the ferromagnetic region where σ depends on both temperature and frequency, while the other at the high temperature region represents the paramagnetic region where σ is only temperature dependent. The point incorporated between the two lines is assigned to the Curie transition point (T_C). Consequently, the first transition can be assigned as (T_{mf}) as it is attributed to the transition between metallic and ferrimagnetic regions and the last one can be assigned as (T_{mp}) as it is due to the transition between paramagnetic and metallic regions.

The values of the activation energies for the ferrimagnetic region (E_I) and the paramagnetic region (E_{II}) were then calculated and represented in Table IV. From the table it is clear that, the values of the activation energies calculated for the ferrimagnetic region is lower than that calculated for the paramagnetic region. In the ferrimagnetic region the most predominant mechanism of conduction is the hopping of electrons between the iron ions of different valences. Accordingly, a small activation energy for this region is obtained. Another hopping process is expected between iron and copper ions. The hopping frequency of each process depends on the content of each element on each site and their ionization energy. The large activation energy of the paramagnetic region indicates that the conduction is mainly due to a small positive polarons which migrate inside the sample under the effect of the large thermal energy due to heating and small internal viscosity of the sample. Also, at the high temperature some Cu^{2+} on the tetrahedral site will be transferred to Cu^{1+} and migrate to its preferential octahedral site leaving positive holes participate in cooperation with the small positive polarons in the conduction process. Generally, the values of activation energy presented in Table IV decrease with the increasing in the cadmium Content except for sample with $x = 0.5$, which can be considered as the critical cadmium concentration. This was in good agreement with the percolation theory of Scholl and Binder [21].

TABLE IV Values of activation energy at applied frequency of 200 kHz for $Cu_{1-x}Cd_xFe_2O_4$ system

Cd content (x)	Activation energy (eV)	
	Ferrimagnetic region (E_I)	Paramagnetic region (E_{II})
0.0	0.514	0.853
0.1	0.460	0.810
0.3	0.432	0.743
0.5	0.529	0.950
0.7	0.365	0.659
0.9	0.332	0.610
1.0	–	0.581

Fig. 6a–c shows typical curves indicate the variation of ε' with absolute temperature at different frequencies. The representative data gives a constant values for ε' in the first temperature region where a small thermal energy given to the sample and no liberation of charge carriers from their localization takes place. After that a progressive increase in ε' was observed until reaching the transition temperature with position depending on the applied frequency and the amount of cadmium in the sample. The presence of frequency dispersion of ε' indicated the short range dependence of conductivity which is in direct correlation with the dielectric

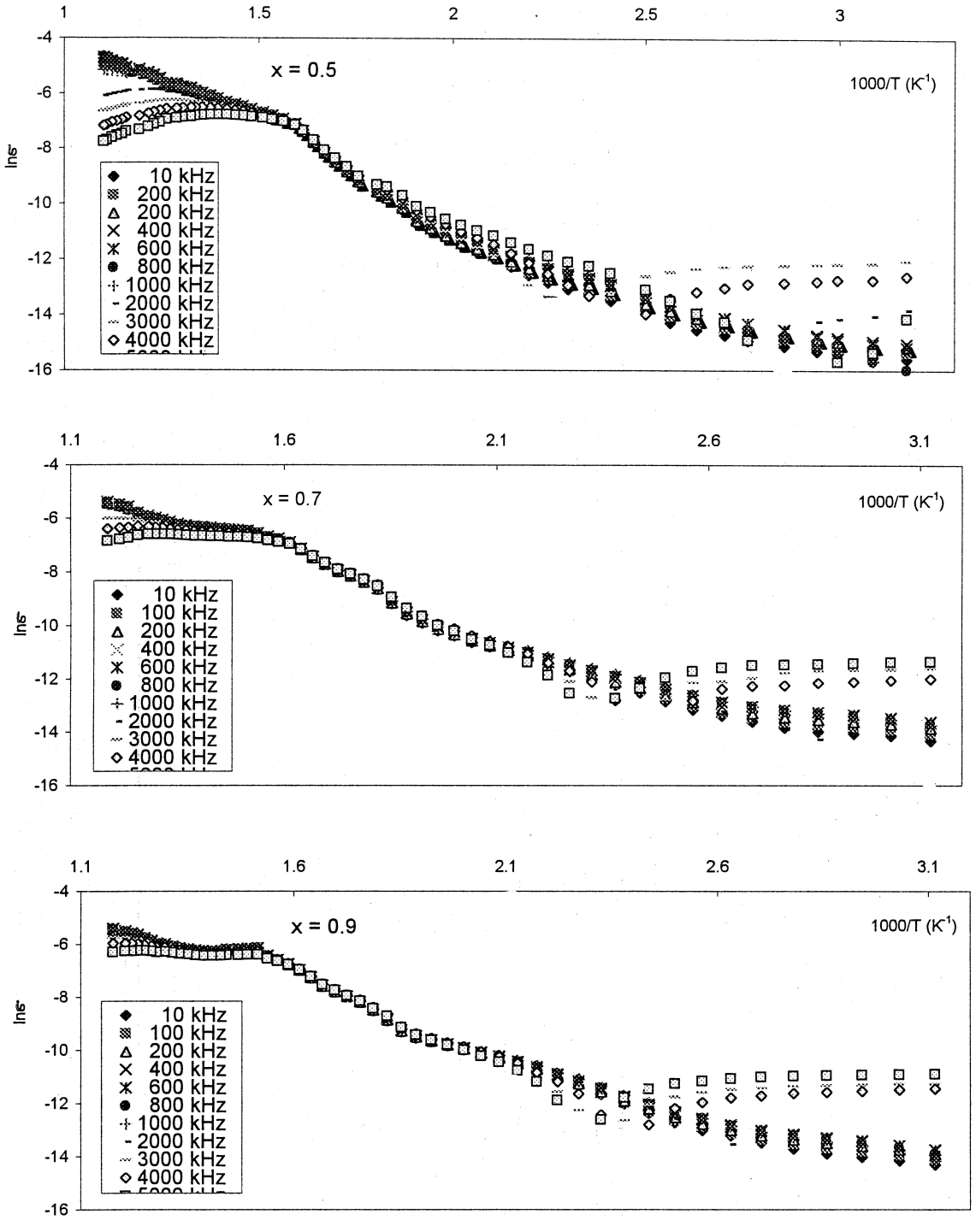

Figure 5 Relation between ln σ and reciprocal of absolute temperature at different Cd content as a function of applied frequency for $Cu_{1-x}Cd_xFe_2O_4$ system.

constant [22]. After this the dielectric constant decrease and then increase again giving rise to a second transition which agrees with the last one obtained in the conductivity data (T_{pm}). On the microscopic scale one can find that the stable region of ε' with temperature indicates the participation of electronic polarization which is independent of temperature. In the second temperature region, the orientation polarization plays a significant role since it is a temperature and frequency dependent. In this region more of the frozen (localized) dipoles will be librated and oriented in the field direction give rise to a maximum value of ε'. The minimum value of ε' indicates the polarization destruction due to high thermal energy. After such destruction some other types of polarization need high thermal energy will participate in the polarization mechanism. The most preferable in this region are the migrational as well as Maxwell Wagner polarization those takes place in the regions separating the grains [21]. The fluctuation of the number of Fe^{2+} between increasing and decreasing is the real and the direct cause but is not completely sufficient on the increase and decrease of ε' with temperature. This is because the e's produced from the valence exchange are responsible for the polarization that takes place in each sample. The decrease in ε' after the second transition is attributed to the large thermal energy which overcome the field effect. In other word, the disordering in the system will be increased and the hopping frequency is decreased. Assuming the cation distribution suggested using the Mössbauer spectroscopy (Table III) it is obvious

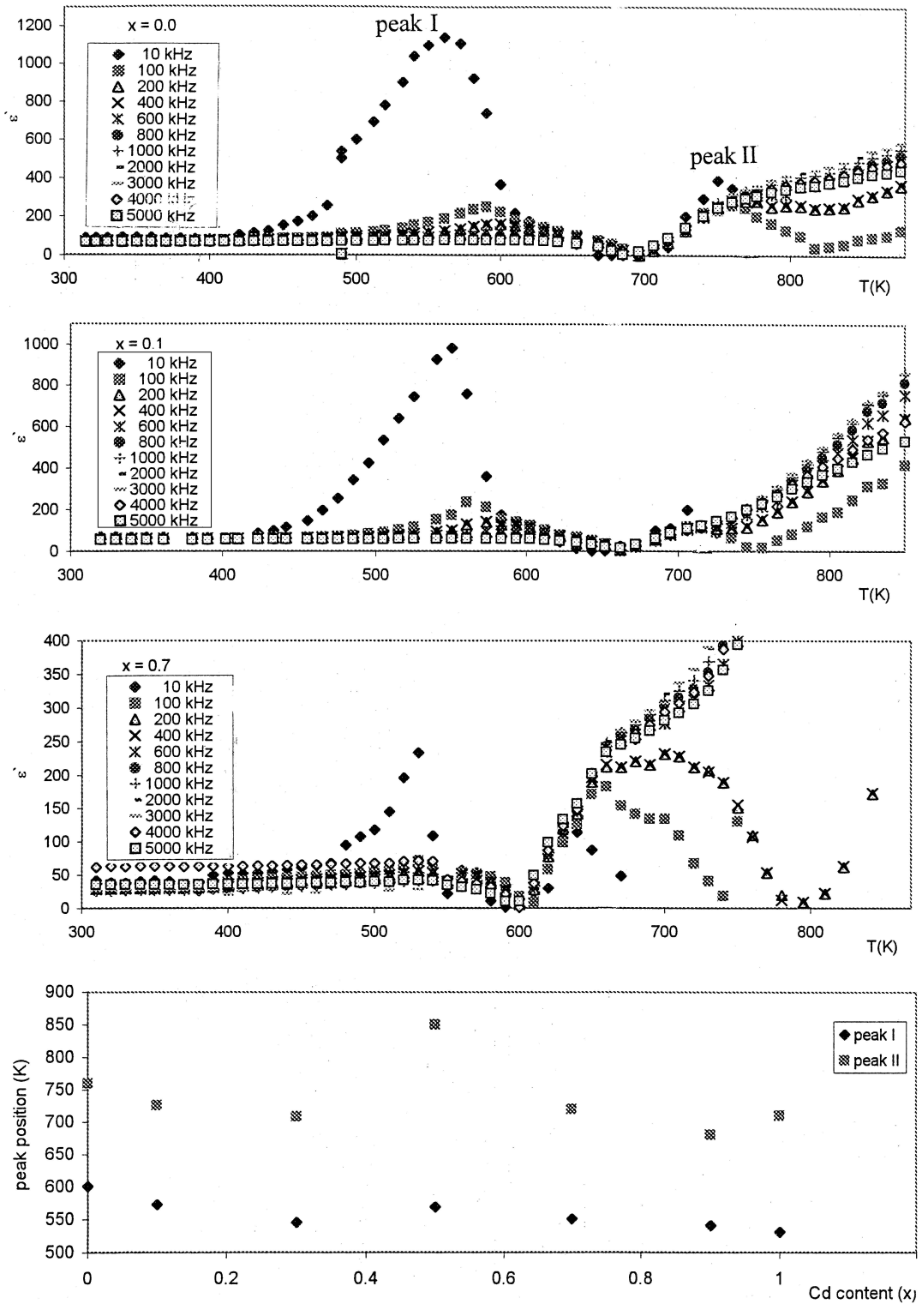

Figure 6 (a) to (c) Relation between dielectric constant and absolute temperature as a function of applied frequency for samples with different Cd-content. (d) Relation between peaks positions and Cd-content (at 200 kHz).

that, Cd^{2+} ions replace the Fe^{3+} on the tetrahedral site and at the same time increase Fe^{3+} on the octahedral site due to their migration. This will increase the conductivity on the octahedral site due to the variation of Fe^{2+}/Fe^{3+} ratio. At $x = 1$, no Cu^{2+} ions exist on the tetrahedral site and cadmium ferrite was obtained in which the activation energy reaches its minimum value (Table IV). Due to the direct correlation between the conductivity and the dielectric constant, one can guess the increase of the latest which agrees will with our experimental data. In the high temperature region the variation of some of Cu^{2+} to Cu^{1+} give a chance to copper ions to exchange valence with iron ions. Accordingly, the dielectric constant and conductivity vary because they are of the same origin.

Fig. 6d describes the peak position vs. cadmium content (x). From the figure it is clear that peaks (I and II) decreases continuously with increasing cadmium content with an exception increase at $x = 0.5$. This means that this concentration again can be considered as the

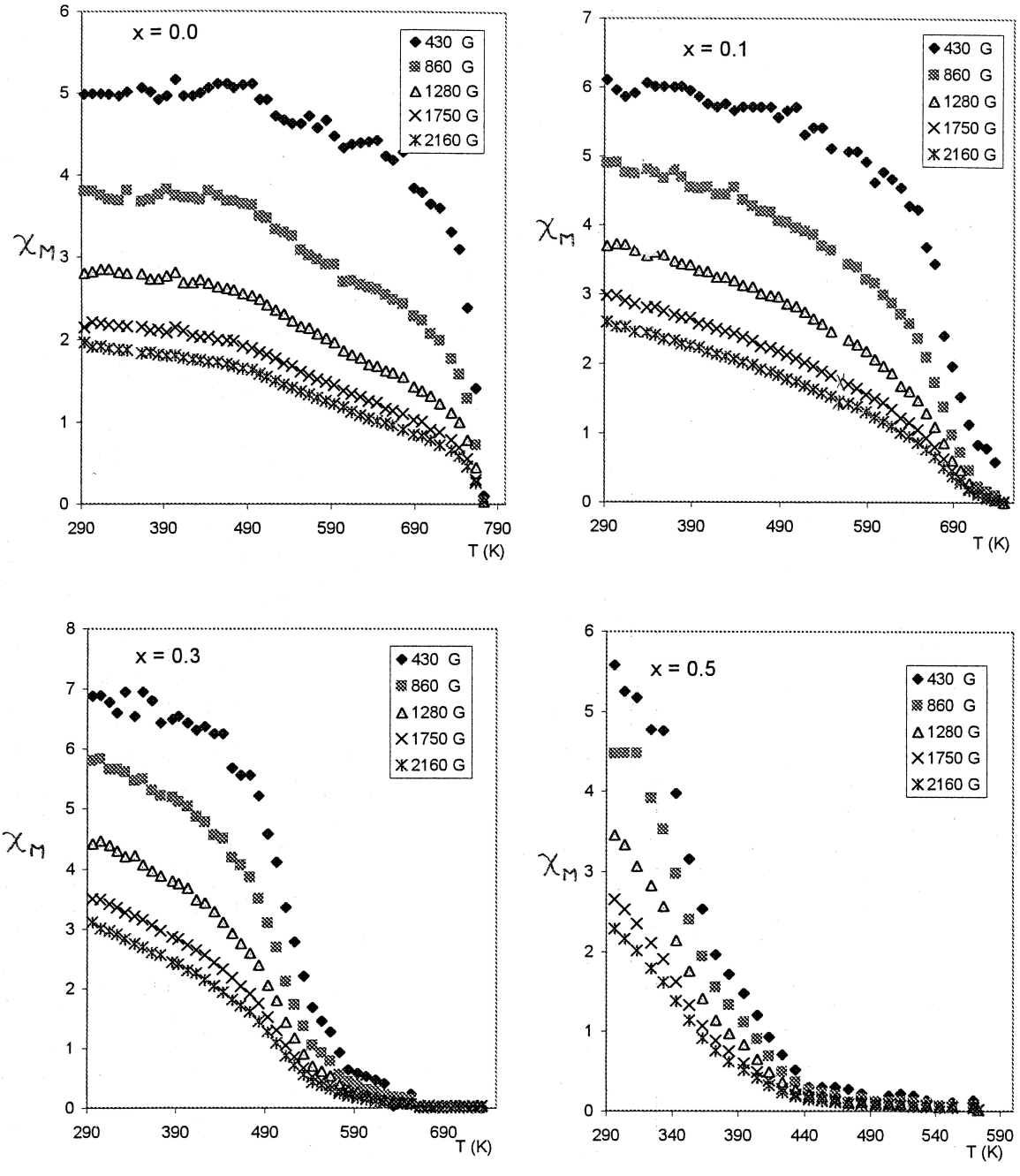

Figure 7 Relation between molar magnetic susceptibility and the absolute temperature as a function of different magnetic field intensities for $Cu_{1-x}Cd_xFe_2O_4$ system.

critical one at which both cadmium ferrite and copper ferrite participates by equal proportions in the polarization mechanism. Mazen *et al.* [3] found that the resistivity of the $Cu_{1-x}Cd_xFe_2O_4$ system prepared by standard ceramic method increases with x to a maximum value near a composition with $x = 0.5$ and then decreases with further increase of x.

3.2.5. Magnetic properties

Fig. 7 shows the molar magnetic susceptibility (χ_M) vs. absolute temperature at different magnetic field intensities for the spinel ferrite $Cu_{1-x}Cd_xFe_2O_4$, $x \leq 0.5$. The general trend of the first three concentrations of cadmium are nearly the same where the magnetic susceptibility was observed to decrease with increasing temperature. The sample with $x = 0.5$ gives nearly paramagnetic behavior except in the first 20 K which shows nearly stable values of χ_M. This was expected because the magnetic ordering is large as well as the ferrimagnetic region in case of small cadmium concentration. The values of the Curie temperature (T_C) which separate the ferrimagnetic and paramagnetic regions, was also decreased from 765 K at $x = 0$ to 439 K at $x = 0.5$ as shown in Table V. This means that by increasing the Cd-content the paramagnetic region (disordered state) is increased on the expense of the ferrimagnetic region. The lowest interaction was obtained at $x = 0.5$ which means that the ferrimagnetic grains are widely separated and enclosed by non-magnetic cadmium ions. The Mössbauer data enhances this point as mentioned before. From the point of view of magnetic field intensity and its effect on the magnetic susceptibility, it is noted that χ_M decreases by increasing the

TABLE V Magnetic data of $Cu_{1-x}Cd_xFe_2O_4$ system at magnetic field intensity of 1280 G

Cd content (x)	T_C (K)	Effective magnetic moment (BM)	
		Observed	Calculated
0.0	765	5.52	4.17
0.1	720	5.24	5.06
0.3	580	4.82	6.28
0.5	439	4.07	9.58

field intensity due to the saturation of the ferromagnetic domains at such high field.

According to the cation distribution estimated using the Mössbauer spectroscopy, the effective magnetic moment (μ_{eff}) can be calculated assuming Equation 6 given below [23]:

$$[5.92\,(1+x+y)+3.0\,(1-x-y)] - [5.92\,(1-x-y)+3.0\,(y)] \quad (6)$$

where, 5.92 and 3.0 μ_B are the magnetic moments of the Fe^{3+} and Cu^{2+} ions, respectively. The values of the effective magnetic moment as well as the observed effective magnetic moment (calculated from the experimental data) are represented in Table V. From the table it is clear that, the values of the observed effective magnetic moment decreases with increasing cadmium content. The direct cause of this behavior is the exchange interaction constant between the different sites where the relative magnitude of $J_{AB} > J_{BB} > J_{AA}$. At $x = 1$, the obtained $CdFe_2O_4$ is a normal spinel type structure in which the Cd^{2+} ions occupy the tetrahedral interstices with no Fe^{3+} ions present. This will cause the presence of the major paramagnetic phase with the small remenance ferrimagnetic one near room temperature [23].

Table V also shows that, the values of μ_{eff} observed at $x = 0$ and 0.1 are larger than that calculated while, at $x = 0.3$ the observed magnetic moment (4.82 BM) is less than calculated one (6.28 BM). This points to the predominant effect of Cd^{2+} ions in the system. At $x = 0.5$ the calculated magnetic moment is larger than twice that of the observed one due to the increase in the exchange interaction of B-site on the expense of that of A-site. Also the small values of the observed moment can be explained in terms of the non-collinear spin arrangement due to the small canting angle of the spins of the B-site with respect to spins of A-site [23].

4. Conclusions

(1) $Cu_{1-x}Cd_xFe_2O_4$ system can be prepared through the thermal decomposition of their respective metal oxalates.

(2) X-ray diffraction of the samples shows single phase cubic spinel except for the sample with $x = 0$ that has a tetragonal structure.

(3) The lattice parameter and X-ray density were found to increase with increasing the Cd content which can be attributed to the larger ionic radius of the heavy Cd atom.

(4) The preference of cadmium ions to reside at tetrahedral site was estimated from increase in the intensity ratios of (220)/(222) and (422)/(222) X-ray diffraction lines with increasing Cd content.

(5) Two dominant FT-IR bands ν_1 and ν_2 attributed to the stretching vibration of Fe^{3+}-O^{2-} in the tetrahedral and octahedral complexes were obtained for all the investigated samples.

(6) The Mössbauer spectra of samples with $x \geq 0.7$ show a paramagnetic doublet while samples with $x \leq 0.3$ exhibit normal Zeeman split sextets. The sample with $x = 0.5$ shows one sextet attributed to the iron ions in the octahedral site. The magnetic hyperfine field was found to decrease with increasing Cd content.

(7) Temperature variation of ac conductivity showed a decrease in the conduction activation energy with increasing Cd content except for sample with $x = 0.5$ which can be considered as critical concentration.

(8) The effective magnetic moment was found to decrease with increasing Cd content due to enclosing of ferromagnetic grains by non-magnetic cadmium ions.

Acknowledgement

The authors would like to thank Dr. A. A. El-Bellihi, Chemistry Department, Faculty of Science, King Abdul Aziz University, Jeddah, KSA, for measuring the DTA-TG experiments.

References

1. A. GOLDMAN, "Modern Ferrite Technology" (Marcel Dekker, NY, 1993).
2. S. A. PATIL, S. M. OTARI, V. C. MAHAJAN, M. J. PATIL, A. B. PATIL, M. K. SOUDAGAR, B. L. PATIL and S. R. SAWANT, *Solid State Commun.* **78** (1991) 39.
3. S. A. MAZEN, B. A. SABRAH, A. A. GHANI and A. A. ASHOUR, *J. Mater. Sci. Lett.* **4** (1985) 479.
4. V. R. KULKARNI and A. S. VAINGANKAR, *J. Mater. Sci.* **22** (1987) 4087.
5. B. P. LADGAONKAR and A. S. VAINGANKAR, *Mater. Chem. Phys.* **56** (1998) 280.
6. M. U. RANA, M. UL-ISLAM and T. ABBAS, *ibid.* **65** (2000) 345.
7. M. UL-ISLAM, T. ABBAS and M. A. CHAUDHRY, *Mater. Lett.* **53** (2002) 30.
8. A. A. CHONI, A. I. ETYHHAND and A. A. MOHAMED, *Proc. Int. Conf. Ferrites* **5** (1980) 216.
9. M. A. GABAL, A. A. EL-BELLIHI and S. S. ATA-ALLAH, *Mater. Chem. Phys.* In press.
10. G. GROSSE, Mos-90, version 2.2, 2nd ed. (Oskar-Maria-Graf-Ring), Munchen (1992).
11. K. V. KUMAR and D. RAVINDER, *Mater. Lett.* **52** (2002) 166.
12. A. COETZEE, D. J. EVE and M. E. BROWN, *J. Therm. Anal.* **39** (1993) 947.
13. EL-H. M. DIEFALLAH, M. A. GABAL, A. A. EL-BELLIHI and N. A. EISSA, *Thermochim. Acta* **376** (2001) 43.
14. International Center for Diffraction Data, JCPDS, PDF2 Data Base, Swarthmore, PA, USA (1996).
15. C. C. WU, S. KUMARAKRISHAN and T. O. MASON, *J. Solid State Chem.* **37** (1981) 144.
16. L. CERVINKA and Z. SIMSA, *Czech. J. Phys.* B **20** (1970) 470.
17. R. D. WALDRON, *Phys. Rev.* **99** (1955) 1727.

18. C. B. KOLEKAR, P. N. KAMBLE and A. S. VAINGANKAR, *Bull. Mater. Sci.* **18** (1995) 133.
19. A. NARAYANASAMY and L. HAGGSTROM, *Solid State Phys.* **16** (1983) 591.
20. Q. M. WEI, J. B. LI and Y. J. CHEN, *J. Mater. Sci.* **36** (2001) 5115.
21. M. A. AHMED and E. H. EL-KHAWAS, *Ind. J. Phys.* **74** (2000) 497.
22. M. S. SELIM, G. TURKY, M. A. SHUMAN and G. A. EL-SHOBAKY, *Solid State Ionics* **120** (1999) 173.
23. A. K. NIKUMBH, A. V. NAGAWADE, V. B. TADKE and P. P. BAKARE, *J. Mater. Sci.* **36** (2001) 653.

Received 15 July
and accepted 30 December 2003